Electromagnetic Pulse Induced Failure Analysis of GaN HEMT Based Power Amplifier

Lei Wang, Changchun Chai, Tian-Long Zhao, *Member, IEEE*, Feng Wei, *Senior Member, IEEE*, Wei-Shen Liu, Yutian Wang, Zhao Li, Le Xu, *Member, IEEE*, Fuxing Li, and Yintang Yang, *Senior Member, IEEE*

***Abstract*—In this article, we first reveal the performance degradation and physical failure mechanism of a lab-designed GaN power amplifier (PA) module based on a commercial GaN high-electron-mobility transistor (HEMT) with high-power electromagnetic pulse injected. We carried out a systematic step pulse injection experiment to hunt out the degradation and failure threshold of PA module by monitoring its S-parameter and the gate-source resister (R_{GS}) of GaN HEMT. Moreover, the performance indexes of GaN PA, including gain, power-added efficiency, output power, and signal-to-noise ratio, have been measured before/after degradation for comparative analysis. The intact surface circuit microscope of PA module and the degradation electrical characteristics of GaN HEMT demonstrated that the GaN HEMT is the vulnerable component of GaN PA. Furthermore, the numerical simulations and decapsulation experiments are carried out for GaN HEMT to gain insight into the failure process and physical failure mechanism. The results reveal that the failure mode is thermal-induced gate metal melting of the GaN HEMT. The failure mechanism is mainly attributable to the impact ionization, which induced by the high pulse voltage under the gate near the source. This is followed by the thermal–electrical feedback state in the device internal until the temperature finally reaching the melting point of the gate metal.**

***Index Terms*—Electromagnetic pulse, failure analysis, GaN, high-electron-mobility transistor (HEMT), power amplifier (PA), reliability.**

I. Introduction

GaN high-electron-mobility transistors (HEMTs) are promising candidates for application in high-voltage, high-frequency, and high-efficiency power electronics fields ascribed to their superior performances, such as high breakdown voltages [1], [2], [3], low on-resistance R_{on} [4], and excellent thermal conductivity [5]. The power converter as a typical GaN HEMT application presents a trend of rapid increase [6] in power electronic systems, featured with the lower switch losses, higher operation frequency, and energy conversion efficiency [7]. Meanwhile, the GaN HEMT also has located itself as an attractive candidate for the high-power amplifier (PA) due to the excellent material properties of GaN. The GaN-based PA possesses improved RF output power compared with traditional Si-based or GaAs-based PA devices [8]. The sustainable development in semiconductor manufacturing technology facilitates the applications of GaN PA in the satellite communication, radar, 5G communication system and communication stations and electronic countermeasure system [9], [10], [11], [12], [13], [14], [15]. In the application of radar communication, the PA module, as the core component of the transmitter, needs to provide hundreds of kilowatts of power in order to make the RF signal radiate to the farther space through the antenna feed [16], which make them subjected to radiate high electromagnetic emissions. Especially in the field of electronic countermeasures, all kinds of interference make the electromagnetic environment of electronic equipment operation is more severe. All these make the reliability of GaN power devices and GaN PA module increasingly concerned.

Research works on the reliability of GaN power devices are very extensive and in-depth, such as dc and RF stress repetitive short-circuit, EDS robustness, and unclamped-inductive switching (UIS) [17], [18], [19], [20], [21], [22], [23]. The RF stress could create bulk traps by hot-electron effects for GaN HEMT, which are located between gate-drain or gate-source and result in a decrease of the output power and drain current [17], [18]. The short-circuit stresses in the p-GaN HEMT will facilitate the trapping and carrier accumulated in gate region and lead to the degradations of electrical parameters [19]. Under ESD pulse condition, the degradation of AlGaN/GaN HEMT on ESD robustness is mainly put down to contact resistivity, inverse piezoelectric effect, temperature, and contact metal migration [20], [21]. The UIS will enlarge the electric field near the drain and result in the increasing the leakage current and high-power dissipation by the inverse-piezoelectric effect. The UIS failure is sensitive to the higher bus voltage and larger load inductance [22], [23].

Recently, the reliability of GaN HEMT under high-power electromagnetic stress has also attracted great attention due

Manuscript received 3 May 2023; revised 31 July 2023; accepted 8 September 2023. Date of publication 15 September 2023; date of current version 6 December 2023. This work was supported in part by the National Nature Science Foundations of China under Grant 61974116, in part by the Fundamental Research Funds for the Central Universities under Grant ZYTS23029, and in part by the Innovation Fund of Xidian University under Grant YJSJ23019. Recommended for publication by Associate Editor J. Popovic-Gerber. *(Corresponding authors: Tian-Long Zhao; Yutian Wang.)*

Lei Wang, Changchun Chai, Tian-Long Zhao, Yutian Wang, Fuxing Li, and Yintang Yang are with the Key Laboratory of the Ministry of Education for Wide Band-Gap Semiconductor Materials and Devices, School of Microelectronics, Xidian University, Xi'an 710071, China (e-mail: lwang2020@stu.xidian.edu.cn; ccchai@mail.xidian.edu.cn; zhaotl@xidian.edu.cn; ytwang@xidian.edu.cn; lifuxing@stu.xidian.edu.cn; ytyang@mail.xidian.edu.cn).

Feng Wei, Wei-Shen Liu, Zhao Li, and Le Xu are with the School of Electrical Engineering, Xidian University, Xi'an 710071, China (e-mail: fwei@mail.xidian.edu.cn; wsliu@stu.xidian.edu.cn; zli@stu.xidian.edu.cn; lexu@mail.xidian.edu.cn).

Color versions of one or more figures in this article are available at https://doi.org/10.1109/TPEL.2023.3315726.

Digital Object Identifier 10.1109/TPEL.2023.3315726

to the harsh operated environment, such as high-power electromagnetic pulse (EMP), high-power microwave (HPM), and high-radiation harsh field. Zhou et al. [24] proposed a thermal breakdown failure mechanism model based on electrothermal simulation for GaN HEMT under a HPM pulse injection. Our research group [25], [26], [27] have studied the failure mechanisms for E-mode and D-mode GaN HEMT device with a high-power EMP injection. The results showed that in addition to the thermoelectric effect, the inverse piezoelectric effect also plays a role due to the piezoelectric properties of GaN materials, and is theoretically verified by numerical models.

Strong electromagnetic energy can lead to module performance degradation or even failure damage by the mean of electromagnetic coupling. However, the past high-power electromagnetic stress reliability on GaN HEMTs is mainly focused on the device level, the reliability of GaN HEMTs-based module (such as PA and LNA) has been rarely reported. This is because the scene of high-power electromagnetic stress acting on module is such a complex process, which increases the difficulty of research. The complexity is reflected in the next two aspects as follows. 1) Electromagnetic energy can be through near-field radiation, far-field radiation, signal lines, power lines, microstrip lines, and other ways from the source of interference to the electronic system. 2) The process of performance degradation and failure mechanism analysis in module involves multidisciplinary knowledge range in circuits, devices, semiconductor materials, and numerical modeling.

Our group has obtained the rich research foundation about the failure analysis under high-power electromagnetic stress of various semiconductor module, such as Si-based CMOS inverter and GaAs-based LNA in numerical simulation and experimental analysis [28], [29]. Based on the abovementioned research, in this article, we convert the complex electromagnetic field into a simple circuit by means of an equivalent alternative method to simplify the interference of the complex electromagnetic field on GaN PA [30]. Then, we independently set up a systematic experimental test platform for EMP injection, and explore the degradation or failure threshold of GaN PA module by monitoring its performance index of Gain, power-added efficiency (PAE), output power, and signal-to-noise ratio. For the first time, the damage progress and failure mechanism of GaN PA under the action of EMP are investigated comprehensive on the basis of experiment platform and simulation technology.

The rest of this article is organized as follows. In Section II, the detailed experimental procedure is described. In Section III, the results of the experiment are fully demonstrated and the failure mechanism is analyzed based on the microstructure after de-cap experiments results and thermal simulation results. Finally, Section IV concludes this article. In short, this article makes the reference for the reliability assessment and design of power modules when using GaN HEMT devices in the power electronics fields.

II. Experiment Setup

The GaN PA was designed based on a commercial depletion-mode GaN HEMT (CGH-27015F) manufactured by Cree, Inc. which is designed specifically for wide bandwidth, high-Gain, and high-efficiency applications. The lab-designed GaN PA module referenced to datasheet is shown in Fig. 1(a) and the enlarged rectangle part is GaN IC packaged with ceramic, as shown in Fig. 1(b). The center frequency of the GaN PA was designed to work on S-band.

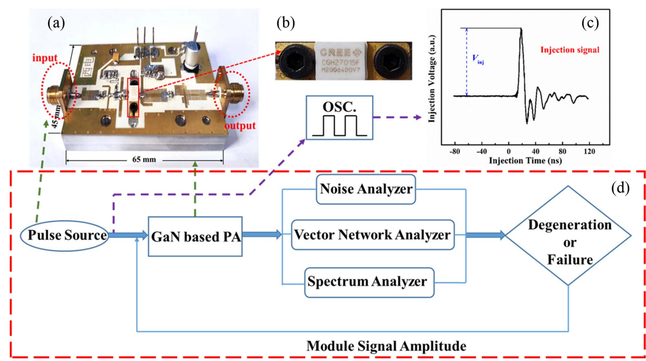

Fig. 1. Flowchart of the proposed test progress.

In this article [16], [17], the behavior of GaN HEMT performances undergoing electromagnetic, RF, dc, and combinations stress has been presented. When pulsed input power generated by an RF generator located at 1 mm above the microstrip line connecting the gate is 40 dBm, a voltage of 1 V is induced at the gate of transistor by using a magnetic probe. Presently, the researchers mostly take the step voltage pulse as the signal model in the study of the damage effect event of the semiconductor device with the EMP event [30]. So in our injection experiment, series of high-voltage pulse signals were adopted to inject into the GaN PA input port, which is equivalent to the EMP coupled into the GaN PA module.

The high-voltage pulse was generated from a self-developed pulse output system consist of a laser (Dawa 300), a high-voltage source (Testman 20 kV), a circuit module that controls the trigger, with the maximum output pulse voltage is 20 kV, pulse current 200 A, pulse width 10∼15 ns. The waveform is shown in Fig. 1(c).

Based on the abovementioned analysis, a complete test setup for GaN PA injection experiments is shown in Fig. 1, and the marked part in the dotted box is the test flowchart, as shown in Fig. 1(d). It consists of three parts as follows.

1) The self-developed pulse source, which can generate an adjustable step voltage pulse signal injecting into the input port of PA.
2) The lab-designed GaN PA module, which is fixed to a cooling plate as the device under test.
3) The test system that includes a noise analyzer to measure the signal to noise ratio characterizing the deterioration of the noise performance of an amplifier, a vector network analyzer to measure S parameter within the operating frequency range, and a spectrum analyzer to measure output power and efficiency of the PA.

When starting the injection experiment, in order to ensure the signal can be injected, the injection times should be two rather than more to avoid cumulative thermal effect; meanwhile, the

pulse voltages are monitored by an oscilloscope in real time. Each time the high voltage source system was triggered, a voltage pulse was injected into the PA input port. At the end of each injection, the S-parameter of the GaN PA was detected by network analyzer (Rohde&Schwarz ZNC3), meanwhile, the R_{GS} of GaN HEMT was also tested to judge the degradation and failure of GaN PA. If there is no degradation of the PA properties, continue increasing the amplitude of the pulse voltage until the gain drops by half.

At this very moment, the signal to noise coefficient (NF), output power, and drain efficiency of the PA are all measured to compare with that of before injection. During characterization testing, the voltages drain-to-source (V_{DS}) of the transistors are bias at 28 V and gate-to-source (V_{GS}) voltages are −2.8 V (I_{DS} = 100 mA).

Continue increasing the injection power until PA is completely failure judging by the gain. In order to investigate possible failure mechanisms, further de-layer experiments, i.e., do away with the ceramic cap from transistor package, have been put into effect, and then the micromorphology was analyzed by the technology of scanning electron microscope (SEM), focused ion beam (FIB) cross section, and energy dispersive X-ray spectroscopy (EDX).

III. Experiment Results and Discuss

A. Degradation and Failure Analysis

Typical electrical parameters of GaN PA module are obtained after every electric pulse signal injection. Fig. 2(a) shows the small signal gain (Gain) at the center frequency of 2 GHz for GaN PA, which is extracted from the S_{21} curve under different injection voltages (V_{in}). The relationship between R_{GS} of GaN HEMT and injection voltage is shown in Fig. 2(b). It can be found that both R_{GS} and Gain are almost unchanged before injection voltage reaching 1200 V, when injection voltage goes up to 1300 V, both R_{GS} and Gain drop off a cliff. The Gain goes down from 14 to 7 dB (extracted at V_{in} = 1300 V), becoming half of that before injection. GaN PA cannot work normally and the parameter Gain cannot be measured after the 1400-V pulse injection. The R_{GS} goes down from 4 MΩ to 4 kΩ (extracted at V_{in} = 1300 V), and then even to 400 Ω (extracted at V_{in} = 1400 V). It can be concluded that the GaN PA failure after the 1300-V pulse injection and maybe completely burned out when the injection voltage reaching 1400 V. Therefore, we defined 1300 V as the failure threshold and 1400 V as the burn-out threshold.

To further confirm this conclusion, the output power, NF, PAE of the GaN PA have also been measured before/after the 1300-V pulse injection and shown in Fig. 3. Fig. 3(a) shows the output power as a function of input power for 2 GHz. Before injection, the output power ranges from 26 to 33 dBm, and that degraded to a range of 21 to 30 dBm after injection. Fig. 3(b) shows the degradation of noise levels NF before/after the 1300-V pulse injection. The NF is a parameter that characterizes the deterioration of the noise performance of an amplifier. The larger the value, the greater the noise added during transmission, and

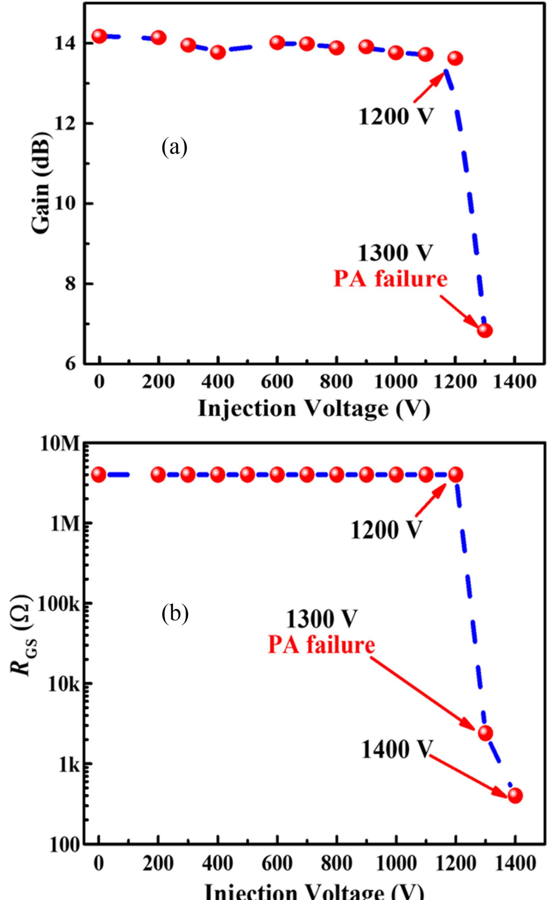

Fig. 2. Relationship between injection voltage and (a) gain. (b) RGS.

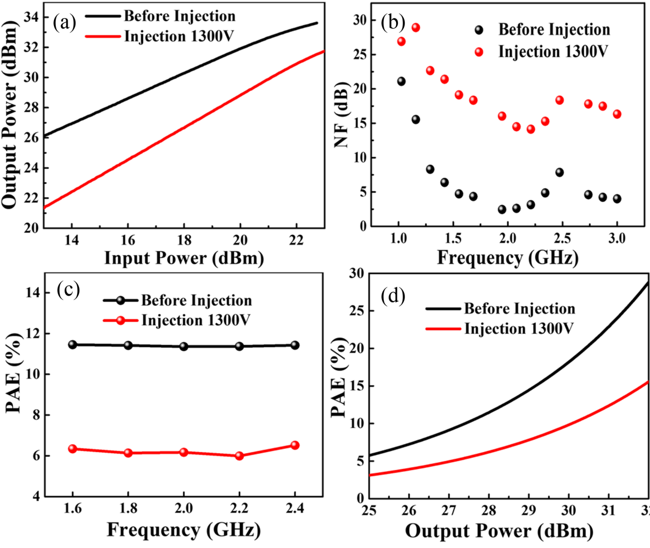

Fig. 3. (a) Relationship between input power and output power. (b) Relationship between frequency and noise figure. (c) Relationship between frequency and PAE. (d) Relationship between output power and PAE.

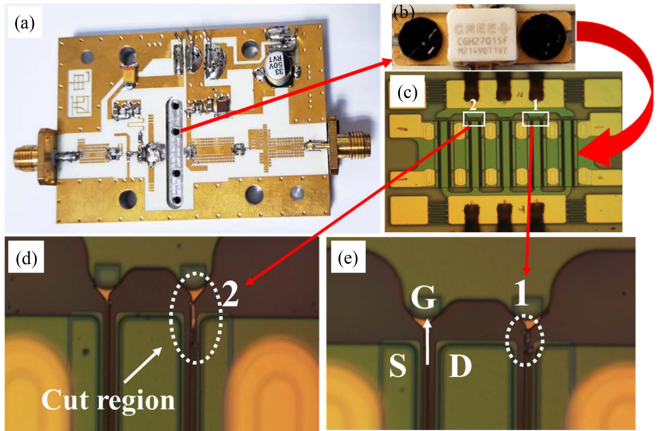

Fig. 4. De-cap failure analysis after injection test.

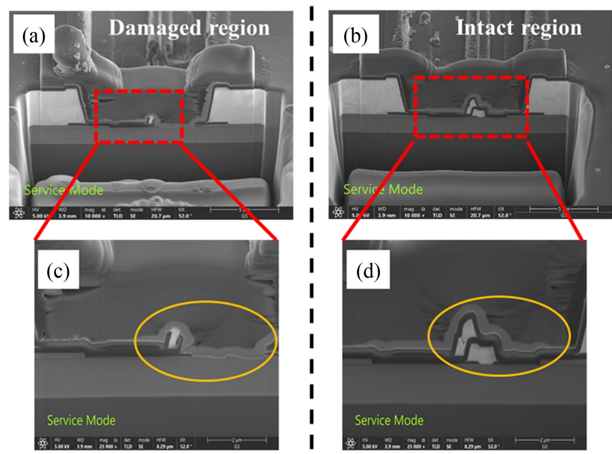

Fig. 5. (a) Title side view of damaged region in GaN HEMT after FIB-SEM. (c) Enlarged view of damaged region. (b) Title side view of intact region in GaN HEMT after FIB-SEM. (d) Enlarged view of damaged region.

vice versa. It can be seen from noise coefficient spectrum range of 1–3 GHz that the noise deteriorates obviously in the whole frequency band, especially at the central frequency of 2 GHz, the NF increases from 2 to 15 dB, which is much higher than the industry standard for GaN PA. Fig. 3(c) and (d) shows the power added efficiency (PAE) as a function of frequency and output power before/after the 1300-V pulse injection. The PAE represents the proportion of dc power converted into RF power, which is a key index of RF PA. It can be clearly noticed that there is a significant decline in conversion efficiency of the GaN PA after injection. Based on the abovementioned PA performance measurement, we can further conclude that the GaN PA failure after the 1300-V pulse injection.

In order to explore the root cause of GaN PA failure, the optical microscope was used to magnify the PA module surface shown in Fig. 4(a). The results indicate that the surface of the whole circuit board including the microstrip line and discrete components emerge no obvious signs of burnout. So we supposed to the failure mechanism may be a consequence of an evolution of the GaN chips internal structure because that the power semiconductor device is usually confirmed the most fragile components in power electronic converters in the view of reliability [31].

To verify this hypothesis, we dissected the GaN HEMT from the PA module, as shown in Fig. 4(b), to test its electrical characteristics. However, the output and transfer characteristics of the GaN HEMT can no longer be measured in the normal operated conditions due to the R_{GS} goes down about 10 000 times (from 4 MΩ to 400 Ω) and the gate loses the ability of controlling the channel after the EMP injection. It can be concluded that the GaN HEMT has been burned out, which is the root cause of GaN PA degradation or failure by EMP injection.

To observe the changes in the internal microstructure, locate the failure area, and further analyze the failure mechanism, the further de-cap operation of the GaN HEMT was carried out by removing of the ceramic encapsulation material on the IC core, exposing the core without compromising the function of the parent chip. Then, the surface was examined with a microscope 500× to local the breakdown area and the results are presented in Fig. 4(c). In the top view, it can be found that the most vulnerable point is near the gate as plotted in white rectangle and the partial enlargement are shown in Fig. 4(d) and (e). The region near the gate was damaged obviously. So far, the final location that caused the GaN PA to fail has been identified.

B. Failure Mode Analysis

There are two mainly failure mode for the reliability on GaN HEMT under high-power electromagnetic stress, electrical-induced failure, and thermal-induced failure. The electrical-induced failure refers to the high electric field introduced by the high-power electromagnetic stress will bring in the electric breakdown or mechanical strain of inverse piezoelectric effect and then cause the device degradation or failure. Under this mode, it is often found the mechanical crack or pit-shape defect in the microstructure. The thermal-induced failure refers to the device degradation or failure caused by the thermal accumulation effects, such as self-heating, avalanche breakdown, and hot carrier emission during the action of the high-power EMP electromagnetic stress. Under this mode, it is often found the phenomena of material melting inside the device rather than just in the device surface. In this study, obvious metal melting phenomenon can be seen in the damage region near the gate shown in Fig. 4(d) and (e). So we preliminarily conclude that the failure mode is thermal-induced failure.

To verify this hypothesis, we used FIB etching techniques as follow as SEM and EDX to perform cross-section observations in specific damage regions, form clear high-resolution images, and identify the material composition imaging. The result for damage region is shown in Fig. 5(a). In order to facilitate the analysis of failure mode, FIB-SEM-EDX was also performed at a location without any damage, and the result is shown in Fig. 5(b). Fig. 5(c) and (d) is partial enlarge images in the dotted boxes at 25 000× magnification. Comparing Fig. 5(c) and (d), it is obvious that the key failure mode for GaN HEMT attribute to the thermal-induced failure rather than the electrical-induced failure since the meltdown of the whole gate and partial field

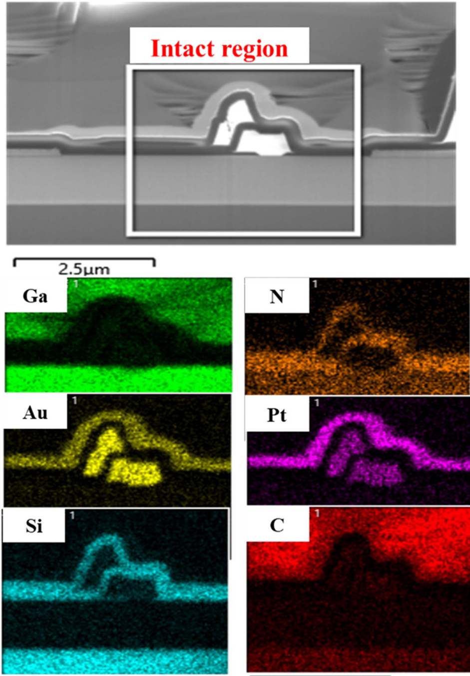

Fig. 6. (a) Title side view of intact region in GaN HEMT where SEM-EDX performed. Different elements are shown in EDX map for Ga, N, Au, Pt, Si, and C.

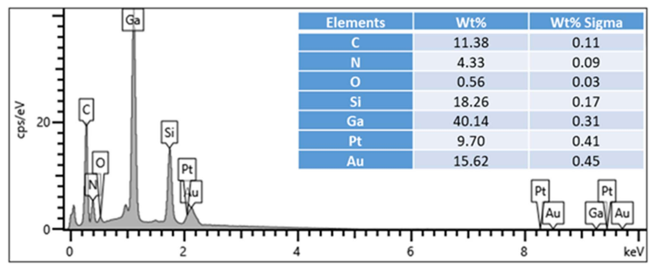

Elements	Wt%	Wt% Sigma
C	11.38	0.11
N	4.33	0.09
O	0.56	0.03
Si	18.26	0.17
Ga	40.14	0.31
Pt	9.70	0.41
Au	15.62	0.45

Fig. 7. Energy dispersive spectrometer results corresponding position of intact region.

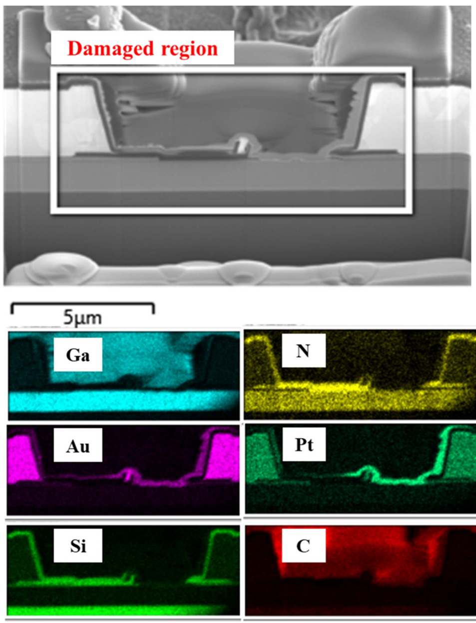

Fig. 8. (a) Title side view of damaged region in GaN HEMT where SEM-EDX performed. Different elements are shown in EDX map for Ga, N, Au, Pt, Si, and C.

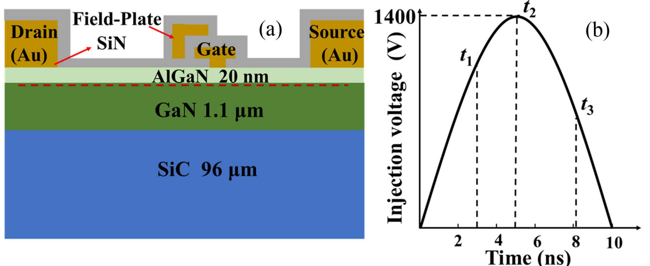

Fig. 9. (a) Cross-section diagram of the GaN HEMT. (b) Injection signal waveform diagram.

plate. In addition, the dielectric between the field plate and gate will be whole breakdown rather than partly for the electrical-induced failure mode.

From the EDX map at the cross section, as shown in Fig. 6, the material of gate and field plate is a composite metal of gold and platinum, and the component of the isolation layer is Si_3N_4. The proportion of different components is shown in Fig. 7 before damaged. Fig. 8 shows the EDX mapping for damaged location and the molten metal moved visibly to the source compared to the intact region. The Si_3N_4 isolation layer is occupied by flowing molten metal, and has undergo a thermal decomposition. At this very moment, Schottky contacts have been destroyed completely, the gate-to-source (drain) resistance reduced sharply, and the gate has lost its ability to control. The output and transfer characteristics of the GaN HEMT can no longer be measured, as discussed previously.

Based on the abovementioned physical failure mode analysis, we conclude that the main failure mechanism of GaN HEMT under EMP is thermal-induced failure caused by high field action. The causes of metal melting need to be further explored and we employ simulation for the process of thermal stress generation with the help of TCAD sentaurus.

IV. Simulation

A. Structural Model

The structure, size, and composition of the device had been obtained by SEM and EDX mapping. Fig. 9(a) shows the schematic cross-sectional structure of the GaN HEMT. The gate-source offset length (L_{GS}), gate length (L_G), and gate-drain offset length (L_{GD}) are 3, 1, and 5 μm, respectively. The total thickness of GaN layer and AlGaN layer is 1.14 μm and the SiC substrate is 96 μm. The source, drain, gate, and field plate contacts are metal layer consist of Au 61.7% and Pt 38.3%. The metal field plate can share the voltage at the gate edge to increase the breakdown voltage of the device. A Si_3N_4 film formed the passivation layer by plasma enhanced chemical vapor deposition and prevented device oxidation by blocking oxygen.

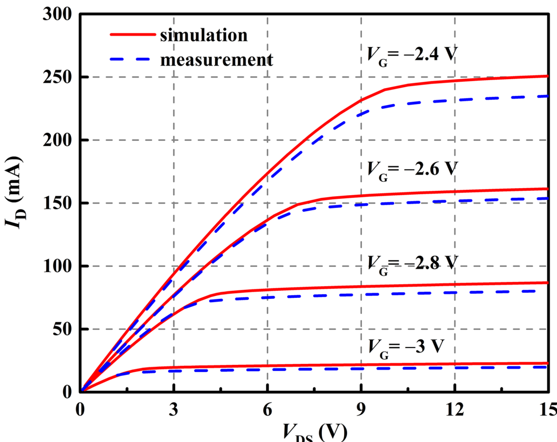

Fig. 10. Output characteristics of GaN HEMT.

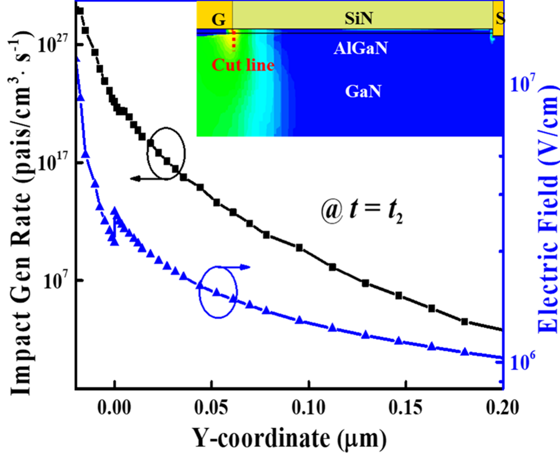

Fig. 11. Extracted impact generate rate along the cut line during EMP injection procedure.

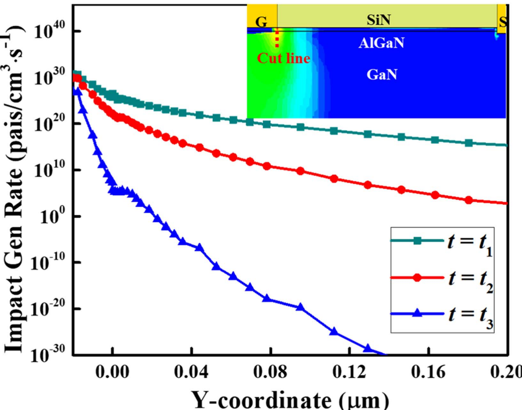

Fig. 12. Extracted impact generate rate and electric field along the cut line.

The source and drain form Ohmic contacts through heavy doping, whereas the gate is Schottky contact. The two-dimensional electron gas exist in the AlGaN and GaN heterojunction interface due to the lattice mismatch of the two materials during the growth process and the dotted line is marked in the Fig. 9(a).

B. Numerical Model

The thermodynamic model [32] due to high-voltage injection into gate electron is activated to simulate the carrier transport progress. In thermodynamic model, the Poisson equation, carrier continuity equations, and heat flow equations are all solved considering the electrical-heating effect inside the device. Moreover, the high-field saturation model that describes mobility degradation in high electric field is applied because the EMP is such a high-voltage signal, as shown in Fig. 9(b). The effect of the internal temperature on the carrier generation–recombination process should be taken into account, so the temperature dependent Shockley–Read–Hall and Auger recombination are applied in our work [33], [34].

In addition, the polarization effects in wurtzite structured GaN are also considered, including spontaneous polarization and strain polarization. The spontaneous polarization results from the center asymmetric nature of wurtzite structure and the strain polarization results from lattice mismatch during heterojunction growth.

In order to verify the correctness of the device model, we present the experiment and simulation output characteristic curves of the device at different gate bias (V_G) ranged from –3 to –2.4 V with the step of 0.2 V and the same drain to source voltage (V_{DS}) from 0 to 15 V. All the experiment and simulation curves display a good consistency, as shown in Fig. 10, demonstrating the correctness of the device model.

C. Simulation Result Analysis

Fig. 11 shows the impact ionization (I.I.) generation rate along the gate edge near the source, perpendicular to the heterojunction interface. The I.I. generation rate and electric field at t_2 along gate edge are given and the peak values are around the corner, and t_1, t_2, and t_3 are shown in Fig. 9(b). The I.I. rate ($\approx 1 \times 10^{30}$ pairs/cm^3·s^{-1}) is largely higher than that in SiC devices ($\approx 1 \times 10^{23}$ pairs/cm^3·s^{-1}), when SiC occur avalanche breakdown [35]. So, it is indicated that the avalanche breakdown occurs within the GaN device. Under the action of high voltage, avalanche I.I. produces large number of charge carriers, which become hot carriers under the action of electric field. The hot carriers induce a large amount of heat inside the device that making the local temperature of the device rise, and the temperature rise was caused by avalanche breakdown.

The I.I. rate decreases gradually, as shown in Fig. 12 from t_1 to t_3, meanwhile, the lattice temperature increases, as shown in Fig. 13 near the gate region. In generally, the high temperature inhibits the generation of collision ionization. Therefore, the reason for the temperature rise in the device cannot be avalanche breakdown, the positive electrothermal feedback should be the main contributor. The electrothermal positive feedback process is as follows. As the temperature increases, the number of carriers increases and the resistivity of the device decreases, which will allow the passage of more current, thus further increasing the device temperature. If the runaway is not stopped soon (usually stopping the power input to the device), the resulting

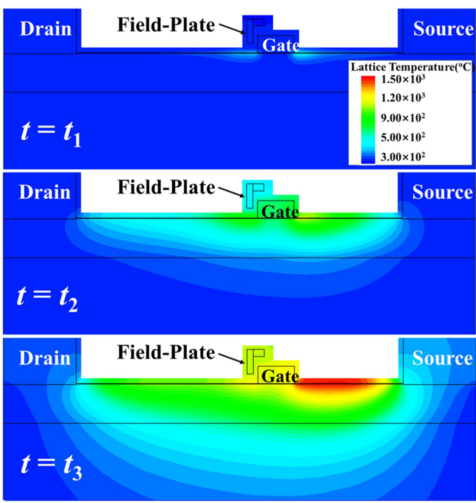

Fig. 13. Lattice temperature distribution during EMP injection procedure.

high temperature will damage or destroy the device. Besides, the inverse-piezoelectric effect may play a role for the failure mechanism by creating dislocations and leading to an increase in leakage current under extremely high electric field between gate and source.

It is noted in Fig. 13 that the temperature is more than 1000 °C at t_3 near the gate metal, reaching the melting point (<1064 °C) of the alloy (Au and Pt), as the melting point of Au is 1064 °C and 1772 °C for Pt [36]. As a result, the gate and field plate region begin to melt and flow towards the source, as is shown in Fig. 5. It also can be seen that the temperature is more than 1500 °C at the isolation layer between gate and source. The Si_3N_4 as the material of isolation layer begin to decomposition from 1500 °C [37] and this result confirms our previous suspicion for the lost isolation layer between gate and source.

V. Conclusion

In this study, the failure analysis of a lab-designed GaN PA under the action of EMP are investigated comprehensive by systematic injection experiment. The failure threshold is confirmed by monitoring the S-parameter of GaN PA and R_{GS} of GaN HEMT. Moreover, the performance indexes of GaN PA, including Gain, PAE, output power, and signal-to-noise ratio, have been conducted before/after degradation for comparative analysis. It is found that the module performance deteriorates obviously when equivalent peak value of pulse voltage reaching 1300 V with the small signal gain reducing to 50% of its original value at the center frequency of 2 GHz and R_{GS} reducing rapidly to 4 kΩ of its original 4 MΩ. Subsequently the R_{GS} quickly decreases to 400 Ω with the peak value of pulse voltage increasing to 1400 V, the gate loses control of the channel and the GaN HEMT are burned out. Therefore, the PA cannot withstand electromagnetic energy in which the equivalent electrical pulse peak value reaching 1300 V and the GaN HEMT is the most vulnerable point in GaN PA which undergoing attacked at first. Furthermore, the numerical simulations and de-capsulation experiments are carried out for GaN HEMT to gain insight into the failure process and physical failure mechanism. De-cap experiments result again verified that GaN HEMT were the most vulnerable part of the GaN PA, and the failure mode was determined to be thermal-induced metal melting at the gate contact in virtue of FIB, SEM, EDX analysis techniques. The simulation results show that the high-voltage injection leading to avalanche breakdown inside the device first, and then the device enters the thermal–electric positive feedback state until the gate metal melt down. This study is an important reference for GaN PA further protection design.

References

[1] Y. Dora, A. Chakraborty, L. Mccarthy, S. Keller, S. P. Denbaars, and U. K. Mishra, "High breakdown voltage achieved on AlGaN/GaN HEMTs with integrated slant field plates," *IEEE Electron Device Lett.*, vol. 27, no. 9, pp. 713–715, Sep. 2006.

[2] E. A. Jones, F. F. Wang, and D. Costinett, "Review of commercial GaN power devices and GaN-based converter design challenges," *IEEE J. Emerg. Sel. Topics Power Electron.*, vol. 4, no. 3, pp. 707–719, Sep. 2016.

[3] J. Millán, P. Godignon, X. Perpiñà, A. Pérez-Tomás, and J. Rebollo, "A survey of wide bandgap power semiconductor devices," *IEEE Trans. Power Electron.*, vol. 29, no. 5, pp. 2155–2163, May 2014.

[4] K. J. Chen et al., "GaN-on-Si power technology: Devices and applications," *IEEE Trans. Electron Devices*, vol. 64, no. 3, pp. 779–795, Mar. 2017.

[5] D. Han, S. Li, Y. Wu, W. Choi, and B. Sarlioglu, "Comparative analysis on conducted CM EMI emission of motor drives: WBG versus Si devices," *IEEE Trans. Ind. Electron.*, vol. 64, no. 10, pp. 8353–8363, Oct. 2017.

[6] W. Qian, J. Lu, H. Bai, and S. Averitt, "Hard-switching 650 V GaN HEMTs in an 800 V DC-grid system with no-diode-clamping active-balancing three-level topology," *IEEE J. Emerg. Sel. Topics Power Electron.*, vol. 7, no. 2, pp. 1060–1070, Jun. 2019.

[7] A. M. Naradhipa, S. Kim, D. Yang, S. Choi, I. Yeo, and Y. Lee, "Power density optimization of 700 kHz GaN-based auxiliary power module for electric vehicles," *IEEE Trans. Power Electron.*, vol. 36, no. 5, pp. 5610–5621, May 2021.

[8] S. S. H. Hsu et al., "Impact of RF stress on dispersion and power characteristics of AlGaN/GaN HEMTs," in *Proc. 24th Annu. Tech. Dig. Gallium Arsenide Integr. Circuit Symposiu*, 2002, pp. 85–88.

[9] S. Mizuno, F. Yamada, H. Yamamoto, M. Nishihara, T. Yamamoto, and S. Sano, "Development of GaN HEMT for microwave wireless communications," *SEI Tech. Rev.*, vol. 74, pp. 71–74, 2012.

[10] F. J. Ortega-Gonzalez, D. Tena-Ramos, M. Patiño-Gomez, J. M. Pardo-Martin, and D. Madueño-Pulido, "High-power wideband L-band suboptimum class-E power amplifier," *IEEE Trans. Microw. Theory Techn.*, vol. 61, no. 10, pp. 3712–3720, Oct. 2013.

[11] H. W. Then et al., "Enhancement-mode 300-mm GaN-on-Si(111) with integrated Si CMOS for future mm-Wave RF applications," *IEEE Microw. Wireless Technol. Lett.*, vol. 33, no. 6, pp. 835–838, Jun. 2023.

[12] Q. Cai, H. Zhu, D. Zeng, Q. Xue, and W. Che, "A three-stage wideband GaN PA for 5G mm-Wave applications," *IEEE Trans. Circuits Syst. II: Exp. Briefs*, vol. 69, no. 12, pp. 4724–4728, Dec. 2022.

[13] J. Zhang, L. Nie, Y. Chen, J. Ren, and S. Ma, "A 6.5-mm^2 10.5–to-15.5–GHz differential GaN PA with coupled-line-based matching networks achieving 10-W peak P_{sat} and 42% PAE," *IEEE Trans. Circuits Syst. II: Exp. Briefs*, vol. 69, no. 11, pp. 4268–4272, Nov. 2022.

[14] B. Cimbili, C. Friesicke, F. van Raay, S. Wagner, M. Bao, and R. Quay, "2.6- and 4-W E-band GaN power amplifiers with a peak efficiency of 22% and 15.3%," *IEEE Microw. Wireless Technol. Lett.*, vol. 33, no. 6, pp. 847–850, Jun. 2023.

[15] J. Wang, Q. Wu, Y. Liu, B. Yan, R. Xu, and Y. Xu, "6–18-GHz high harmonic suppression GaN power amplifier MMIC for integrated electronic warfare systems," *IEEE Microw. Wireless Technol. Lett.*, vol. 33, no. 8, pp. 1183–1186, Aug. 2023.

[16] S. Khemiri, M. Kadi, and A. Louis, "Reliability study of AlGaN/GaN HEMT under electromagnetic, RF and DC stress," *Microelectronics Rel.*, vol. 51, no. 9, pp. 1783–1787, 2011.

[17] N. Moultif et al., "Reliability assessment of AlGaN/GaN HEMTs on the SiC substrate under the RF stress," *IEEE Trans. Power Electron.*, vol. 36, no. 7, pp. 7442–7450, Jul. 2021.

[18] S. Ganguly et al., "DC and RF reliability assessment of 5G-MMW capable GaN HEMT process," in *Proc. IEEE Int. Rel. Phys. Symp.*, 2022, pp. 11B.5-1–11B.5-6.
[19] S. Li et al., "Understanding electrical parameter degradations of P-GaN HEMT under repetitive short-circuit stresses," *IEEE Trans. Power Electron.*, vol. 36, no. 11, pp. 12173–12176, Nov. 2021.
[20] B. Shankar and M. Shrivastava, "Unique ESD behavior and failure modes of AlGaN/GaN HEMTs," in *Proc. IEEE Int. Rel. Phys. Symp.*, 2016, pp. EL-7-1–EL-7-5.
[21] J.-H. Lee et al., "Incorporation of a simple ESD circuit in a 650V E-mode GaN HEMT for all-terminal ESD protection," in *Proc. IEEE Int. Rel. Phys. Symp.*, 2022, pp. 2B.3-1–2B.3-6.
[22] C. Zhang et al., "Unclamped-inductive-switching behaviors of p-GaN HEMTs at cryogenic temperature," *IEEE Trans. Power Electron.*, vol. 37, no. 10, pp. 11507–11510, Oct. 2022.
[23] S. Liu et al., "Single pulse unclamped-inductive-switching induced failure and analysis for 650 V p-GaN HEMT," *IEEE Trans. Power Electron.*, vol. 35, no. 11, pp. 11328–11331, Nov. 2020.
[24] L. Zhou et al., "Investigation on failure mechanisms of GaN HEMT caused by high-power microwave (HPM) pulses," *IEEE Trans. Electromagn. Compat.*, vol. 59, no. 3, pp. 902–909, Jun. 2017.
[25] L. Wang, C.-C. Chai, F.-X. Li, Y. Qin, and Y.-T. Yang, "Influence of gate voltage dependent piezoelectric polarization on damage effect of GaN HEMT induced by high power electromagnetic pulse," *Microelectronics Rel.*, vol. 136, 2022, Art. no. 114665.
[26] Y. Qin, C. Chai, F. Li, Q. Liang, H. Wu, and Y. Yang, "Study of self-heating and high-power microwave effects for enhancement-mode p-gate GaN HEMT," *Micromachines*, vol. 13, no. 1, p. 106, 2022.
[27] L. Wang, C. Chai, T. Zhao, F. Li, Y. Qin, and Y. Yang, "Mechanical-electrical synergy damage effect on GaN HEMT under high-power microwave," *Sci. China Technol. Sci.*, vol. 66, no. 8, pp. 2373–2380, 2023.
[28] Y.-Q. Liu et al., "Physics-based analysis and simulation model of electromagnetic interference induced soft logic upset in CMOS inverter," *Chin. Phys. B*, vol. 27, no. 6, 2018, Art. no. 068505.
[29] F. Li et al., "Study on high power microwave nonlinear effects and degradation characteristics of C-band low noise amplifier," *Microelectronics Rel.*, vol. 128, 2022, Art. no. 114427.
[30] X. W. Xi, C. C. Chai, Y. Liu, Y. T. Yang, Q. Y. Fan, and C. L. Shi, "Analysis of the damage threshold of the GaAs pseudomorphic high electron mobility transistor induced by the electromagnetic pulse," *Chin. Phys. B*, vol. 25, no. 8, 2016, Art. no. 088504.
[31] S. Yang, A. Bryant, P. Mawby, D. Xiang, L. Ran, and P. Tavner, "An industry-based survey of reliability in power electronic converters," *IEEE Trans. Ind. Appl.*, vol. 47, no. 3, pp. 1441–1451, May/Jun. 2011.
[32] G. Lebon, H. Machrafi, M. Grmela, and C. Dubois, "An extended thermodynamic model of transient heat conduction at sub-continuum scales," *Proc. Roy. Soc. A: Math., Phys. Eng. Sci.*, vol. 467, pp. 3241–3256, 2011.
[33] M. S. Tyagi and R. Van Overstraeten, "Minority carrier recombination in heavily-doped silicon," *Solid-State Electron.*, vol. 26, no. 6, pp. 577–597, 1983.
[34] H. Goebel and K. Hoffmann, "Full dynamic power diode model including temperature behavior for use in circuit simulators," in *Proc. 4th Int. Symp. Power Semicond. Devices Int. Continence Soc.*, 1992, pp. 130–135.
[35] J. Wei, S. Liu, S. Li, J. Fang, T. Li, and W. Sun, "Comprehensive investigations on degradations of dynamic characteristics for SiC power MOSFETs under repetitive avalanche shocks," *IEEE Trans. Power Electron.*, vol. 34, no. 3, pp. 2748–2757, Mar. 2019.
[36] S. Inasawa, M. Sugiyama, and Y. Yamaguchi, "Laser-induced shape transformation of gold nanoparticles below the melting point: The effect of surface melting," *J. Phys. Chem. B*, vol. 109, no. 8, pp. 3104–3111, 2005.
[37] C. Greskovich and S. Prochazka, "Stability of Si_3N_4 and liquid phase(s) during sintering," *J. Amer. Ceram. Soc.*, vol. 64, no. 7, pp. C-96–C-97, 1981.

Lei Wang received the B.S. degree in physics from the Hebei Normal University of Science and Technology, Qinhuangdao, China, in 2011, and the M.S. degree in materials physics and chemistry from Shandong University, Jinan, China, in 2014. She is currently working toward the Ph.D. degree in electronic science and technology with the School of microelectronics, Xidian University, Xi'an, China.

Her research interests include the reliability of semiconductor devices and integrated circuits, and protection design.

Changchun Chai received the B.S. degree in microelectronics and solid-state electronics from Tsinghua University, Beijing, China, in 1983, the M.S. degree in microelectronics and solid-state electronics and the Ph.D. degree in electronic science and technology from Xidian University, Xi'an, China, in 1990 and 2005, respectively.

His research interests include semiconductor devices and reliability of integrated circuits, semiconductor devices technology, and design for integrated circuits.

Tian-Long Zhao (Member, IEEE) was born in Jinan, Shandong, China, in 1988. He received the B.S. and Ph.D. degrees in physics from Shandong University, Jinan, China, in 2011 and 2016, respectively.

He is currently an Associate Professor and with the School of Microelectronics, Xidian University, Xi'an, China. His research interests include the reliability of semiconductor devices and reliability of integrated circuits.

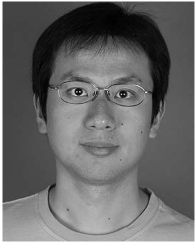

Feng Wei (Senior Member, IEEE) was born in Shaanxi, China, in 1978. He received the B.Eng., M.Eng., and Ph.D. degrees in electrical engineering from Xidian University, Xi'an, China, in 2001, 2004, and 2009, respectively.

From 2004 to 2006, he was a radio frequency (RF) Engineer with ZTE Corporation, Shenzhen, China. From 2013 to 2014, he was a Visiting Scholar with the Commonwealth Scientific and Industrial Research Organization, Canberra, ACT, Australia. Since 2009, he has been with the Collaborative Innovation Center of Information Sensing and Understanding and the National Key Laboratory of Antennas and Microwave Technology, Xidian University, as a Lecturer and an Associate Professor. He has authored or coauthored more than 50 international and regional refereed journal articles. His research interests include the design of microwave components, circuits, and RF identification systems.

Dr. Wei was a Reviewer for the IEEE TRANSACTIONS ON MICROWAVE THEORY AND TECHNIQUES and IEEE MICROWAVE AND WIRELESS COMPONENTS LETTERS.

Wei-Shen Liu was born in Liaoning, China. He received the B.Eng. degree from the School of Physics and Optoelectronic Engineering, Xidian University, Xi'an, China, in 2021, where he is currently working toward the master's degree in electrical engineering with the Electronic Engineering School.

His research interests include the design of balanced filter power divider and RF amplifier.

Yutian Wang, received the B.S. degree from the Hefei University of Technology, Hefei, China, in 2007, the M.S. degree from South China Normal University, Guangzhou, China, in 2010, and the Ph.D. degree from the Dresden University of Technology, Dresden, Germany, in 2015, all in electrical engineering.

He is currently an Associate Professor with Xidian University, Xi'an, China. His research interests include application and protection of semiconductor devices.

Zhao Li was born in Shaanxi, China. He received the B.Eng. and M.Eng. degrees in electrical engineering from Xidian University, Xi'an, China, in 2020 and 2023, respectively.

His research interests include the design of balanced filter and RF circuit.

Le Xu (Member, IEEE) received the B.S. and M.Eng. degrees in microwave telecommunication engineering, in 2002 and 2005, respectively, and the Ph.D. degree in radio physics, in 2009, all from Xidian University, Xi'an, China.

He is currently an Assistant Professor with the School of Electronic Engineering, Xidian University. He is instructing several courses for undergraduate students, such as electromagnetic field and microwave technology. From 2013 to 2014, he was a Visiting Scholar with the Poly-Grames Research Center, École Polytechnique, University of Montréal, Montreal, QC, Canada. His research interests include computational electromagnetic, physical optics method, and finite-difference time-domain method. He is also interested in the application of computational electromagnetics techniques to problems in engineering.

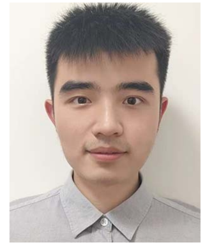

Fuxing Li received the B.S. degree in microelectronics science and engineering from Chongqing University, Chongqing, China, in 2018. He is currently working toward the Ph.D. degree in electronic science and technology from Xidian University, Xi'an, China.

His research interests include the microwave effect and device reliability of hybrid integrated circuits.

Yintang Yang (Senior Member, IEEE) received the B.S. and M.S. degrees in semiconductor devices and microelectronics from Xidian University, Xi'an, China, in 1982 and 1984, respectively.

He was the Professor and Advisor of Ph.D. candidates. He successively held the posts of the Director of the Research Institute of Microelectronics, the Deputy Dean of the School of Technical Physics, the Dean of the School of Microelectronics, and the Vice President of Xidian University. His research interests include energy harvesting IC design, ultralow-power IC design, mixed signal processing, and IC design.

Mr. Yang won the title of National Model Teacher and was a recipient of the Chinese Youth Science and Technology Award.